A 3-D Brownian dynamics simulator for the study of ion permeation through membrane pores. Supporting Info

Claudio Berti,[*,†,‡] Simone Furini,[¶] Dirk Gillespie,[†] Dezső Boda,[§] Robert S. Eisenberg,[†] Enrico Sangiorgi,[‡] and Claudio Fiegna[‡]

Department of Molecular Biophysics and Physiology, Rush University Medical Center, Chicago, Illinois, U.S.A., ARCES and DEI, University of Bologna and IUNET, Cesena, Italy, Department of Medical Biotechnologies, University of Siena, Siena, Italy, and Department of Physical Chemistry, University of Pannonia, Veszprém, Hungary

E-mail: Claudio_Berti@rush.edu

1 Assessment of Brownian dynamics implementation

We checked our Brownian dynamics (BD) implementation by considering the simple case of bulk electrolytes. We considered a cubic simulation domain (100 Å $\times$ 100 Å $\times$ 100 Å) with periodic boundaries filled by an ionic solution (no membrane or channel are present) and an electric field

[*]To whom correspondence should be addressed
[†]Department of Molecular Biophysics and Physiology, Rush University Medical Center, Chicago, Illinois, U.S.A.
[‡]ARCES and DEI, University of Bologna and IUNET, Cesena, Italy
[¶]Department of Medical Biotechnologies, University of Siena, Siena, Italy
[§]Department of Physical Chemistry, University of Pannonia, Veszprém, Hungary

$\mathbf{E}_z$ is applied along the z direction. $\mathbf{E}_z$ produces a net ionic current that can be described by the Nernst-Planck equation. In this case, since ionic concentrations are constant throughout the simulation domain, the flux, of the ν-th ionic species is:

$$\mathbf{J}_\nu = -D_\nu \frac{z_\nu e C_\nu}{kT} \mathbf{E}_z \tag{1}$$

where D_ν, z_ν, and C_ν are the diffusion coefficient, the valence, and the concentration of the ν-th ionic species, respectively. Figure S1(a) shows the currents as functions of the electric field $\mid \mathbf{E}_z \mid$ obtained for a NaCl solution at different concentrations: 50 mM (top), 100 mM (center) and 200 mM (bottom). The good agreement between simulation (symbols) and theoretical (lines) results confirms that the simulator describes the ionic currents correctly. Analogous results were obtained for different electrolytes over a wide range of concentrations, applied fields and simulation box sizes (data not shown).

In equilibrium, the ions' velocities should follow a Maxwellian distribution:[1–3]

$$f(v_\nu) = \sqrt{\frac{2}{\pi}\left(\frac{m_\nu}{kT}\right)^3}\, v_\nu^2 \exp\left[\frac{-m_\nu v_\nu^2}{2kT}\right] \tag{2}$$

where v_ν and m_ν are the velocity and the mass of the ν-th ionic species, respectively. Figure S1(b) shows the velocity distributions obtained from BD simulations of 100 mM NaCl bulk solution with no electric field applied ($\mathbf{E}_z = 0$). Simulation results (circles and diamonds) match those predicted by Equation 2 (lines). For different ionic mixtures, in the range of concentrations up to $\sim$3 M, much larger than typical physiological environment, the match between simulation results and theoretical results still holds (data not shown).

When an electric field is applied, the velocity distribution becomes a displaced Maxwellian.[4] Figure S1(c) shows the distributions of the z-component of the velocity (v_z) of Na^+ ions for different applied voltages ($\mathbf{E}_z$ ranges from 0 to 10^{10} V/m, corresponding to 100 V applied along z). Although voltages larger than 1 V ($\mid \mathbf{E}_z \mid = 10^8$ V/m in this case) are unphysical in an aqueous

electrolyte (water molecules split), the displacement of the curves is visible at these values. This results is in agreement with the fundamental calculations of Eisenberg et al. on the basis of the full Langevin equation. They showed that the velocity distribution contains an asymmetric term that is proportional to the ionic flux. This asymmetric term corresponds to the shift seen in Figure S1(c). This is true even in the high friction limit.[4]

As an additional confirmation of the correct simulation of the behavior of the interacting ions, we analyzed the ions' mean square displacement (MSD) for a homogeneous solution with no electric field applied. For a given ionic species ν, it can be computed by:[1–3]

$$\mathrm{MSD}_\nu(t) = \left\langle \mathbf{r}_\nu^2(t) \right\rangle = \left\langle \frac{1}{N_\nu} \sum_{i=1}^{N_\nu} (\mathbf{r}_i(t) - \mathbf{r}_i(0))^2, \right\rangle \tag{3}$$

where $\langle ... \rangle$ denotes averaging over all the N_ν ions of species ν, t is time, and $\mathbf{r}_i(t) - \mathbf{r}_i(0)$ is the vector distance traveled by a given ion over the time interval t. In electrolytes, the MSD increases linearly with time. The slope of the MSD, considered for long time intervals, is related to the diffusion coefficient D_ν. Theoretically, the mean square displacement should obey the following relation:

$$\mathrm{MSD}_\nu(t) = 6 \frac{kT}{m_\nu \gamma_\nu} t = 6 D_\nu t \ , \tag{4}$$

being γ_i and D_i related to each other through the Einstein relation:

$$D_\nu = \frac{kT}{m_\nu \, \gamma_\nu} \ , \tag{5}$$

where k and T are the Boltzmann constant and the temperature, respectively.[5–8] Figure S2 shows the comparison between the MSD obtained for Na^+ (green diamonds) and Cl^- (red circles) from simulations and the predicted slopes obtained with Equation 4 (black and blue lines, respectively). The good agreement confirms that the simulator accurately describes ions in bulk electrolytes. Simulated values are averaged over samples of 100 mM NaCl bulk solution in a cubic simulation

domain (100 Å $\times$ 100 Å $\times$ 100 Å) with periodic boundary conditions. Similar results have been obtained for different ionic mixtures in different concentrations (data not shown).

1.1 Comparison with Dynamic Monte Carlo

The assessment of our BD implementation with bulk solutions test cases is crucial, in our view, to obtain reliable simulation results. Nevertheless, the previous tests do not guarantee that ion motion in ion channels (where ion crowding and electrostatic interactions become critical issues) is correctly described. No theoretical results are available in this case, but a comparison between simulation results obtained for the same channel model with different methods is a good test-bed and a double-check for all the methods involved in the comparison.

The *OX* model (See Figure 1(b) in the main manuscript) of L-type calcium channel (with pore radius equal to 4 Å) has been previously used by Rutkai et al. to investigate binding affinity and dynamic selectivity with the Dynamic Monte Carlo (DMC) technique.[9] Binding selectivity is defined by the ion concentration profile in the channel, while dynamic selectivity is defined by ion flux. Thus, we checked BD simulation results in terms of both binding affinity and dynamic selectivity with those in reference.[9] In this test series we imposed a total concentration of cations (Na^+ and Ca^{2+}) of 100 mM in the left bath and changed the Ca^{2+} mole fraction. The solution in the right bath had 0 M ion concentration. Concentration imbalance between either side of the membrane determines a driving force that allows ions to flow through the channel.

Figure S3 shows the occupancies (upper curves) and flux (lower curves) ratios of Ca^{2+} and Na^+ as functions of the Ca^{2+} mole fraction. For this model calcium channel, binding affinity is always larger than dynamical selectivity. The good agreement between BD and DMC results is a strong consistency double-check for both types of simulation.

The agreement between BD and DMC data holds for ion concentration profiles inside the pore for calcium (Figure S4(a)) and sodium (Figure S4(b)) at different Ca^{2+} mole fractions. At any considerable Ca^{2+} mole fraction value, a Ca^{2+} ion occupies the center of the selectivity filter. The

Ca^{2+} density in this binding site is substantially independent of the Ca^{2+} mole fraction. On the other hand, an increase of Ca^{2+} produces a noticeable increase of calcium density in the remainder of the pore. Analogous results were obtained for different Ca^{2+} mole fractions (data not shown). Na^{+} density profiles in the pore decrease more evenly from left to right and their magnitude decreases everywhere along the pore axis as the Ca^{2+} mole fraction increases. In this case, 1 μs BD simulations are not able to reproduce the DMC results perfectly due to the small number of Na^{+} ions inside the channel. Longer simulations should provide better statistical accuracy.

1.2 Ionic currents variance

It is common practice in BD to provide currents averaged over different realizations of the same system and adding standard deviation/standard error. To determine how long an ion channel simulation should be, in order to provide converged results, we studied the variance of ion current for 10 different realizations of the same system: *OX* configuration, no dielectrics, 100 mM NaCl on both sides, 100 mV transmembrane potential. Figure S5 shows the currents of the different realizations (thin lines), average current (red bold line) and the currents' standard deviation (black bold line) as functions of the simulated time. After $\sim$250 ns the average current becomes stable, but the variance is still large ($\sim$5.3 pA, 15.6% of the average current). The standard deviation decreases as the simulated time increases, reaching 0.862 pA (2.5% of the average current) at $\sim$5 μs of simulated time. Thus, in this case, a single simulation run can give accurate results on ion currents provided that simulated time is at least 5 μs. Similar results have been obtained for other models of Figure 1(b) in the main manuscript. Therefore, we chose 5 μs as a lower limit to simulated time in every run.

1.3 Position-dependent diffusion coefficient

An ion's mobility in membrane pores is believed to be significantly smaller than in bulk solution.[10–12] To test this aspect of ion permeation in our implementation, we used a position-dependent diffusion coefficient $D_\nu(z)$ for each ionic species ν. Outside the channel its value is kept constant to the bulk value D^*_ν. In the channel it is a function of the channel radius ($R(z)$) through the scaling factor α:

$$D_\nu(z) = D^*_\nu \left(\alpha + (1-\alpha) \frac{R(z) - R_{MIN}}{R_{MAX} - R_{MIN}} \right). \tag{6}$$

$D_\nu(z)$ varies smoothly from D^*_ν where the channel radius is maximum (R_{MAX}) to αD^*_ν where the channel radius is minimum (R_{MIN}). The inherent variable of the Langevin equation, however, is not $D_\nu(z)$, but $\gamma_\nu(z)$ that are related through the Einstein relation (Equation 3 in the main manuscript). This relation, strictly speaking, is valid only in the baths, where the high friction limit is satisfied. The relation between $\gamma_\nu(z)$ and $D_\nu(z)$ in crowded environments will be discussed in future works.

We performed a set of simulations, with α ranging from 1 to 0.1, for the *OX* configuration (Figure 1(b) in the main manuscript). The left and right baths contained 100 mM NaCl solution and the transmembrane potential was 100 mV (left to right). α affected only the diffusion coefficient of permeating ions (Na^+ and Cl^-) while it was not applied to structural $O^{1/2-}$ charges.

A lower α produces a smaller mobility and, thus, a larger accumulation of ions in the pore. The smaller α is, the larger the number of Na^+ ions in the pore (Figure S6, red line). However, this dependence is very weak: a 10-fold reduction of α causes an increment of $<5\%$ in the total number of Na^+ ions in the pore. On the other hand, Na^+ current is severely altered by the scaling factor α. In particular Na^+ currents are scaled by the same factor α (Figure S6, black line).

Figure S7 shows the distribution (a), the velocity (b) and the flux (c) of Na^+ ions in the pore for different values of α. The plots are averages over the 2 μs of the simulation. Ion density in the pore is essentially the same for different values of α (as seen in the average number of Na^+

in the pore in Figure S6). On the other hand, the average Na^+ velocity along the pore is highly influenced by the scaling vector α: larger values of α produce larger velocities. The difference is more visible in the channel vestibules, while in the selectivity filter, where α has a smaller impact. Na^+ fluxes show a linear dependence of ion current on the scaling factor α.

To evaluate ion density, velocity and flux profiles we divided the simulation domain into a number of slices with 1 pm width along z. The ion density was the time-averaged number of ions in each slice. The flux was the average net number of ions that crossed the boundary between two neighboring slices. Finally, the velocity was the ratio between the flux and the ion density.

1.4 Computational efficiency

To give an idea of the computational resources required, we provide information about the computation time for the systems we studied. We ran all the simulations on a single core of an Intel Xeon CPU x5365 3 GHz processor. For the *OX* configuration, with no dielectric forces ($\varepsilon_M = \varepsilon_W = 80$) and an average number of ion of 48.79 it took $\sim$2.5 hour to simulate 100 ns. For the same system, with dielectric forces ($\varepsilon_M = 10$, $\varepsilon_W = 80$) and an average number of ion of 50.21 it took $\sim$3.3 hour to simulate 100 ns. The extra time required is due to the computation of dielectric forces.

References

(1) Sprackling, M. *Thermal Physics*; Macmillan physical science; American Institute of Physics, 1991.

(2) Reif, F. *Fundamentals of Statistical and Thermal Physics*; McGraw-Hill series in fundamentals of physics; Waveland Press, 2008.

(3) Li, S. C.; Hoyles, M.; Kuyucak, S.; Chung, S.-H. Brownian Dynamics Study of Ion Transport in the Vestibule of Membrane Channels. *Biophys. J.* **1998**, *74*, 37 – 47.

(4) Eisenberg, R. S.; Klosek, M. M.; Schuss, Z. Diffusion as a chemical reaction: Stochastic trajectories between fixed concentrations. *J. Chem. Phys.* **1995**, *102*, 1767–1780.

(5) Einstein, A. *Investigations on the theory of Brownian movement*; Dover Publications: New York, N.Y, 1956.

(6) Kramers, H. Brownian motion in a field of force and the diffusion model of chemical reactions. *Physica* **1940**, *7*, 284 – 304.

(7) Schuss, Z. *Theory and applications of stochastic differential equations*; Wiley Series in Probability and Statistics - Applied Probability and Statistics Section; Wiley, 1980.

(8) van Gunsteren, W.; Berendsen, H. Algorithms for brownian dynamics. *Mol. Phys.* **1982**, *45*, 637–647.

(9) Rutkai, G.; Boda, D.; Kristóf, T. Relating Binding Affinity to Dynamical Selectivity from Dynamic Monte Carlo Simulations of a Model Calcium Channel. *J. Phys. Chem. Lett.* **2010**, *1*, 2179–2184.

(10) Noskov, S. Y.; Im, W.; Roux, B. Ion Permeation through the α-Hemolysin Channel: Theoretical Studies Based on Brownian Dynamics and Poisson-Nernst-Plank Electrodiffusion Theory. *Biophys. J.* **2004**, *87*, 2299 – 2309.

(11) Comer, J.; Aksimentiev, A. Predicting the DNA Sequence Dependence of Nanopore Ion Current Using Atomic-Resolution Brownian Dynamics. *J. Phys. Chem. C* **2012**, *116*, 3376–3393.

(12) Mamonov, A. B.; Kurnikova, M. G.; Coalson, R. D. Diffusion constant of K^+ inside Gramicidin A: A comparative study of four computational methods. *Biophys. Chem.* **2006**, *124*, 268 – 278.

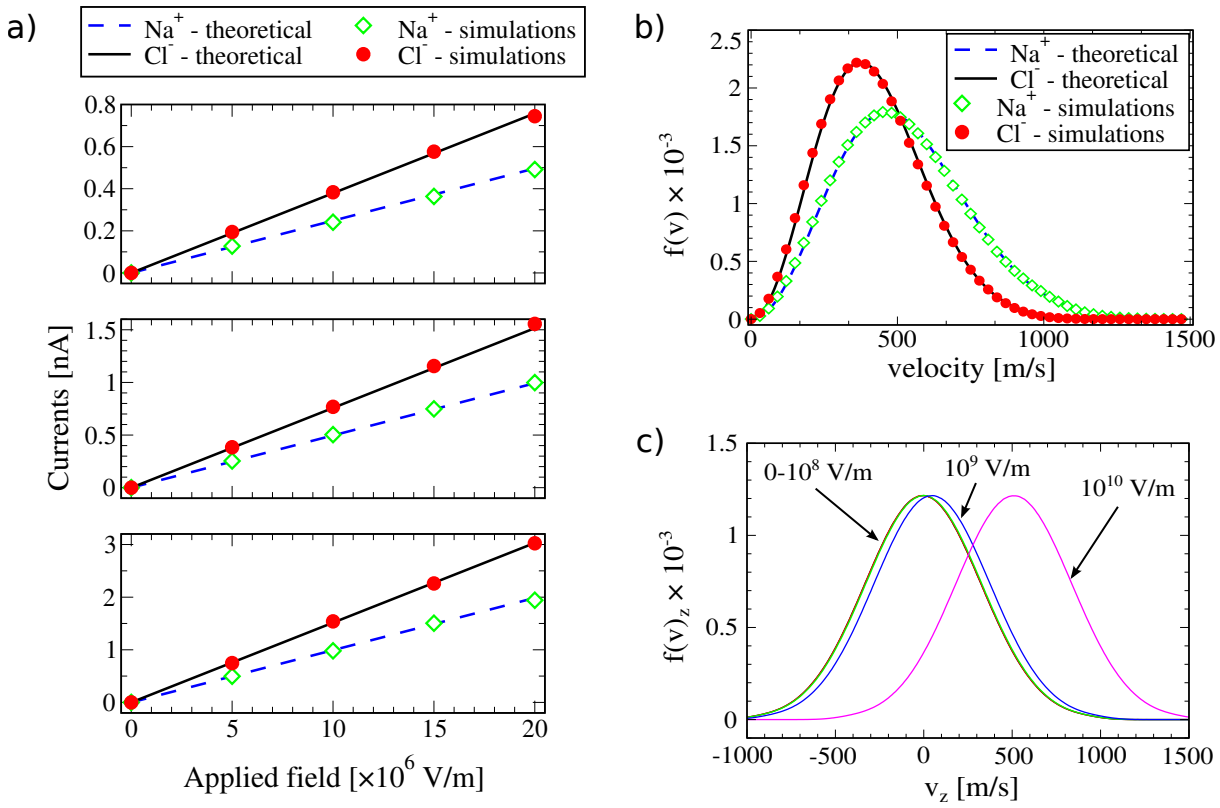

Figure S1: BD algorithm test for bulk NaCl electrolyte (analogous results have been obtained for other electrolytes, data not shown). Simulated currents are in excellent agreement with theoretical results predicted by the NP equation for different values of the electric field $\mid \mathbf{E}_z \mid$ applied along z (a). When $\mathbf{E}_z = 0$, ion velocity distribution follows the Maxwellian distribution predicted theoretically (b). Distribution of the z-component of ions' velocities for values of $\mid \mathbf{E}_z \mid$ (c).

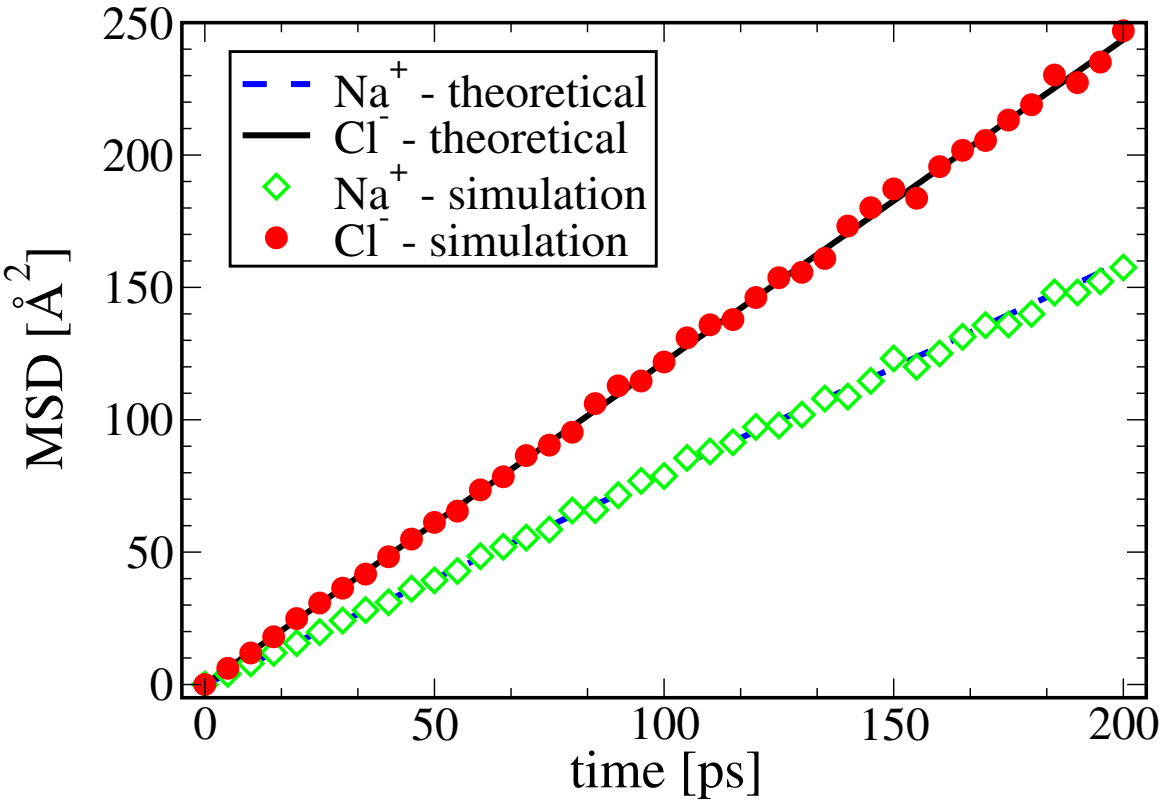

Figure S2: Mean square displacement computed for bulk electrolyte is in good agreement with theoretical predictions.

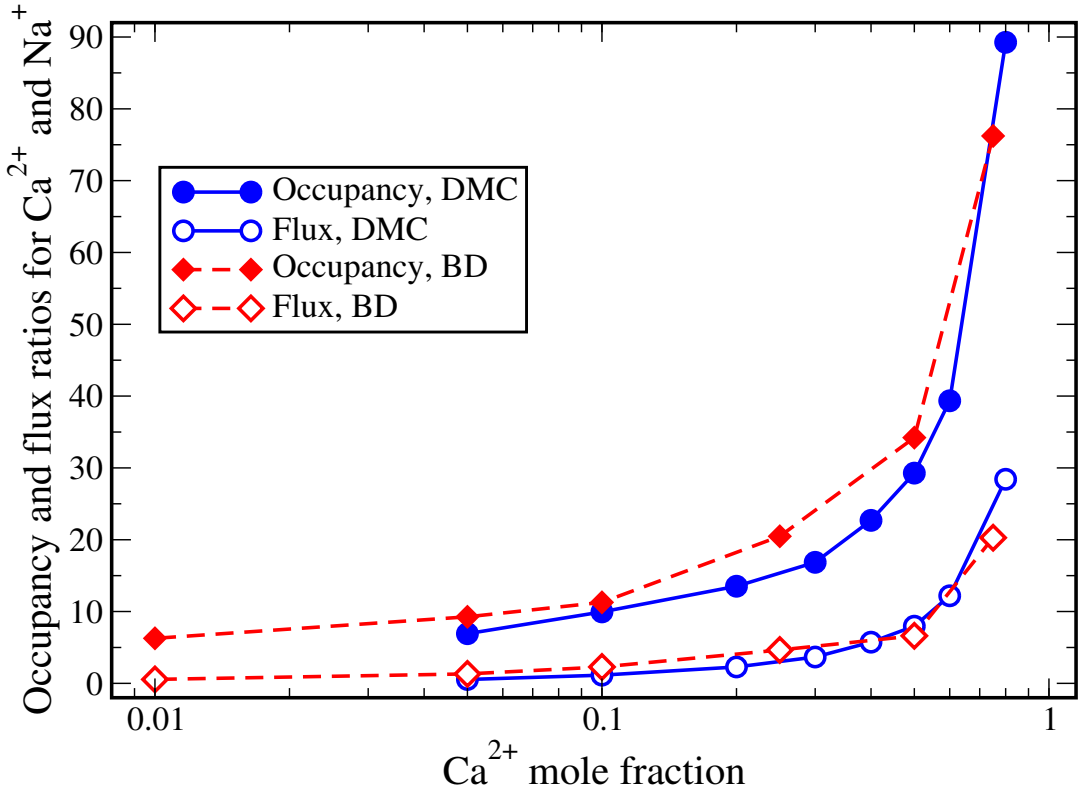

Figure S3: BD-DMC comparison for the calcium channel model *OX* (see Figure 1(b) in the main manuscript) (with 4 Å pore radius). Occupancy and flux ratios for Ca^{2+} and Na^{+} as a function of Ca^{2+} mole fraction for both BD and DMC (a). The two methods are in excellent agreement.

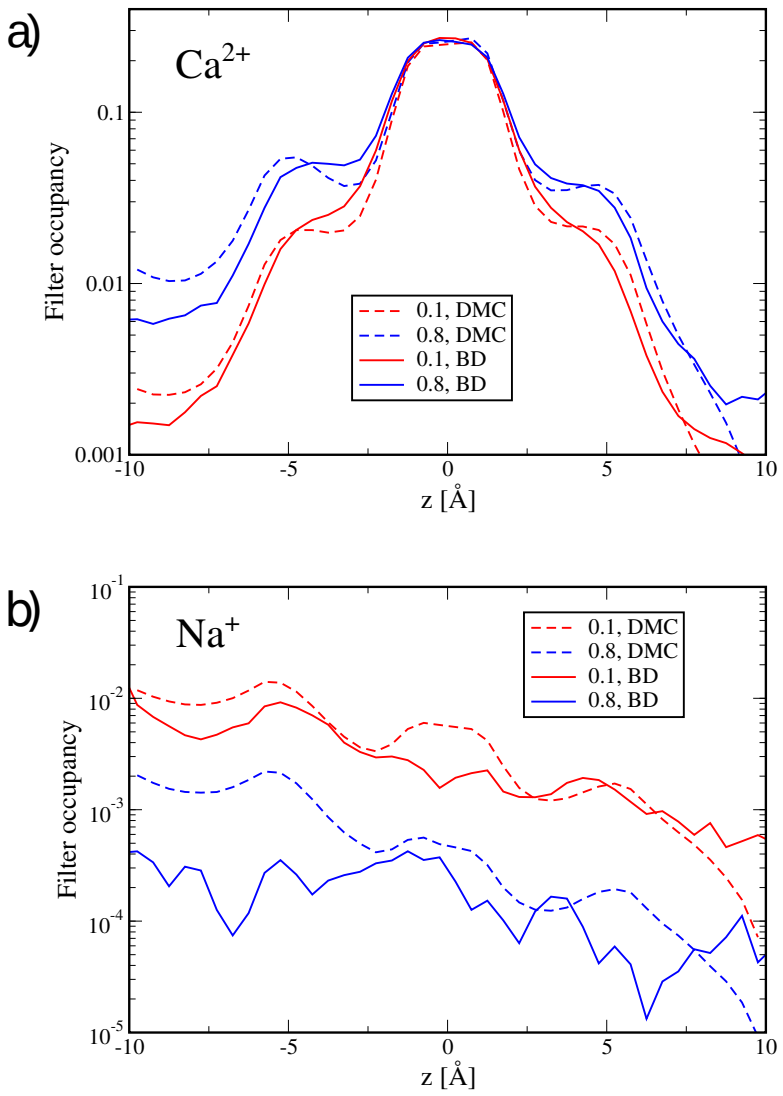

Figure S4: BD-DMC comparison for the calcium channel model *OX* (see Figure 1(b) in the main manuscript) (with 4 Å pore radius). BD and DMC provide very similar results for filter occupancy of Ca^{2+} (b) and Na^{+} (c) for the indicated Ca^{2+} mole fractions, too.

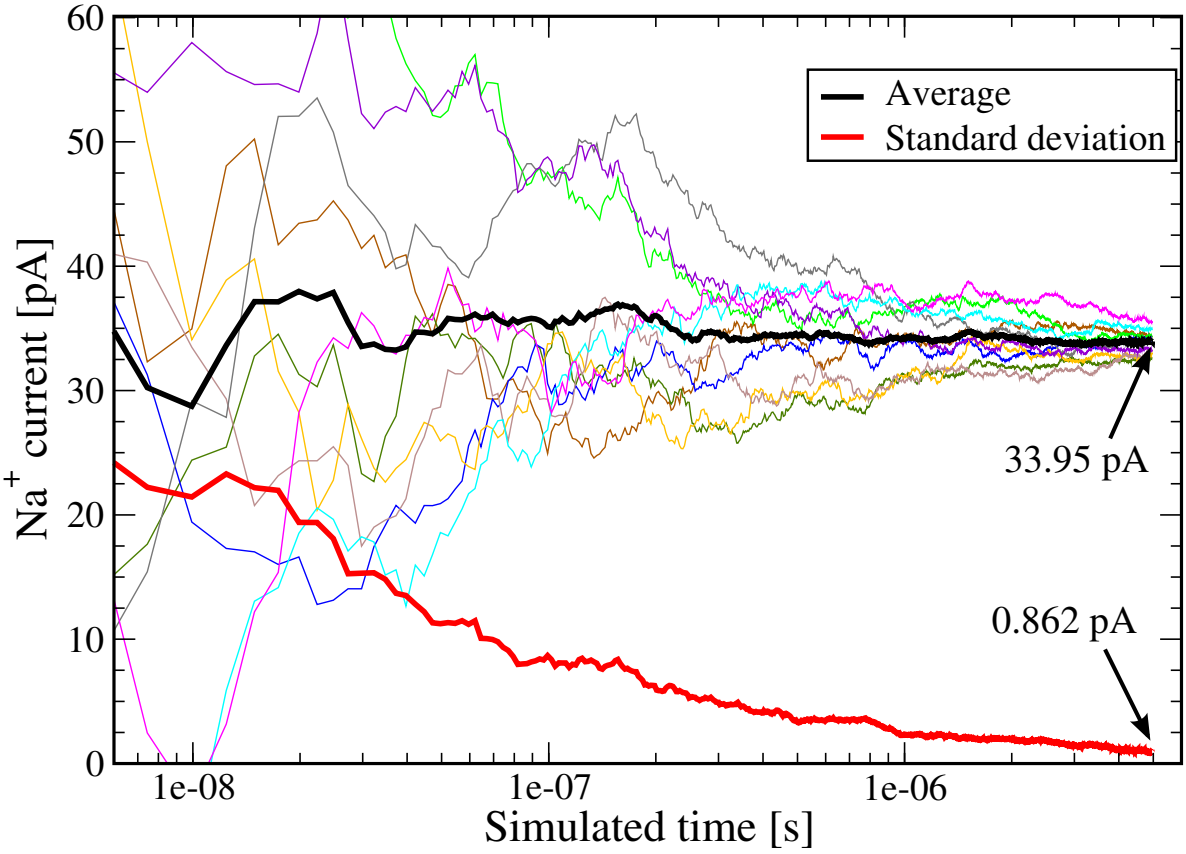

Figure S5: Average and standard deviation of the currents obtained by 10 different realizations of the *OX* configuration (see Figure 1(b) in the main manuscript). At $\sim$5 μs, the standard deviation (red bold line) reaches 2.5% of the average current (black bold line). The currents of the different realizations are displayed with thin lines.

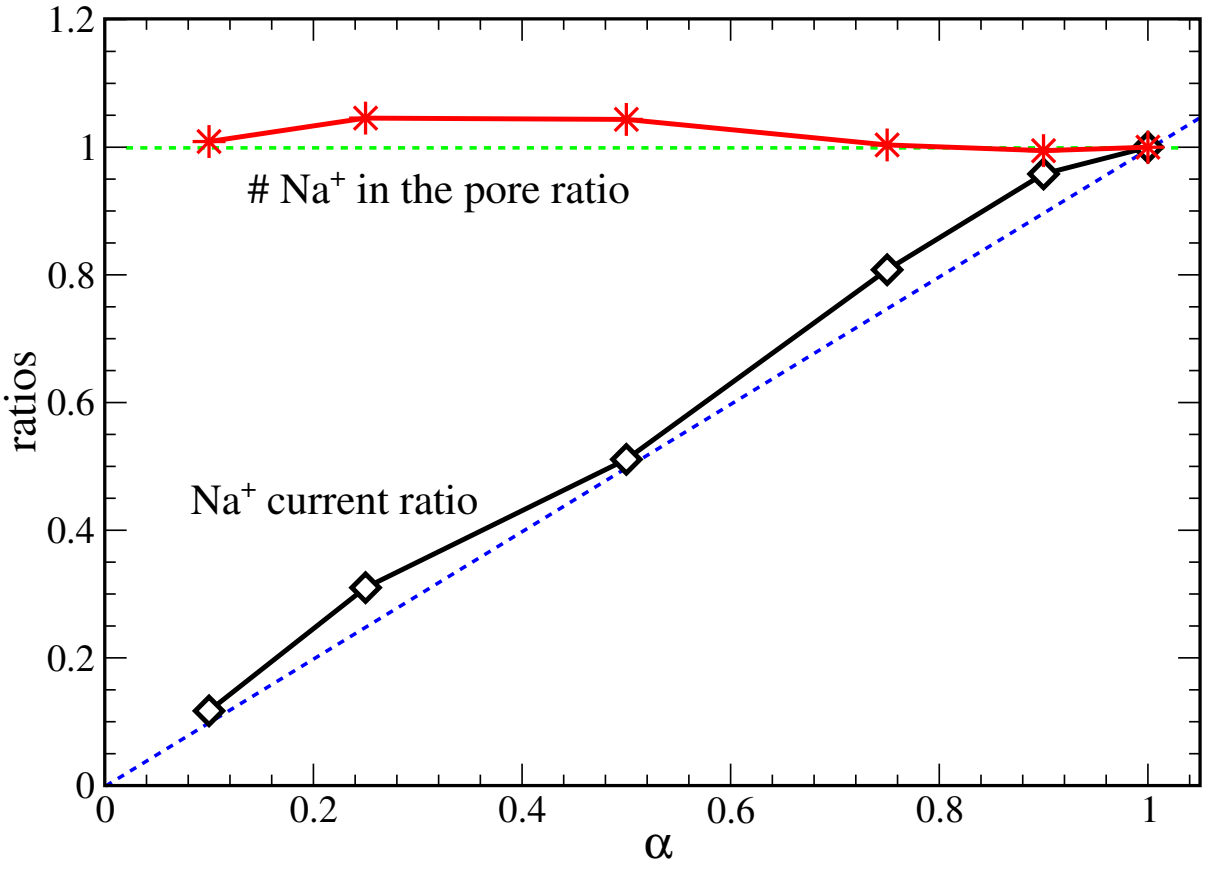

Figure S6: Average number of Na^+ ions in the pore (red) and Na^+ currents (red) for different values of α parameter. Curves are normalized to the values obtained for α=1. Green and blue dashed lines help to note the small dependence of the total Na^+ in the pore and the linear dependence of Na^+ currents with respect to α, respectively.

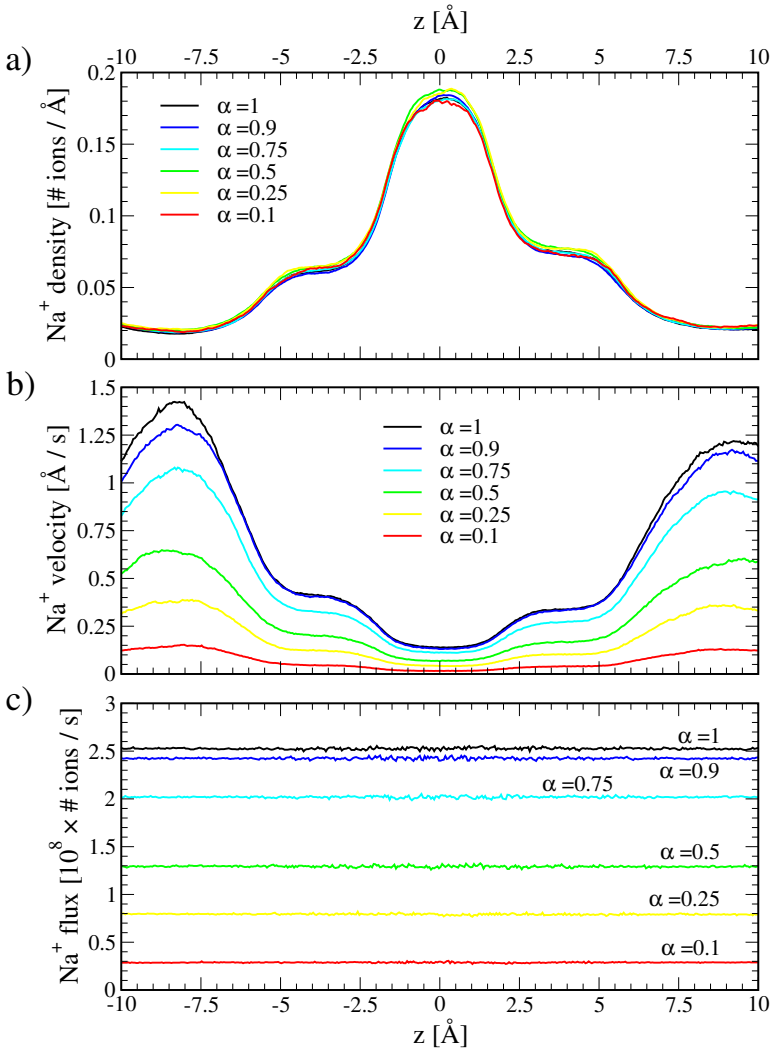

Figure S7: Average Na^+ density (a), Na^+ velocity (b) and flux (c) for different values of α parameter for the *OX* configuration (see Figure 1(b) in the main manuscript).